Dickson-Charge-Pump-Based Voltage-to-Time Conversion for Time-Based ADCs in 28-nm CMOS

ALI ESMAILIYAN [1]**, JIANGLIN DU** [1] **(Member, IEEE),**
TEERACHOT SIRIBURANON [1] **(Senior Member, IEEE),**
FILIPPO SCHEMBARI [1,2] **(Member, IEEE),**
AND ROBERT BOGDAN STASZEWSKI [1] **(Fellow, IEEE)**

[1]School of Electrical and Electronic Engineering, University College, Dublin 4, D04 Ireland

[2] Huawei Research Center, 20090 Segrate, Milan, Italy

The editor coordinating the review of this article was Q. Li.

CORRESPONDING AUTHOR: J. DU (e-mail: jianglin.du@ucdconnect.ie)

ABSTRACT This article demonstrates a digitally friendly time-based analog-to-digital converter (ADC) exploiting Dickson charge-pump (CP) as part of a voltage-to-time conversion (VTC) implemented in 28-nm CMOS. In the proposed technique, the Dickson CP generates a ramp signal that is compared with the input voltage to generate a pulse of commensurable widths, which is then fed to a D-type flip-flop (DFF)-based time-to-digital converter (TDC). The TDC is composed of CMOS DFFs and digital circuits for digital conversion without any use of analog-intensive circuits, e.g., amplifiers or current sources. Thanks to the robustness of Dickson CP characteristics, the digital outputs of the proposed ADC can be corrected through a low-complexity deterministic digital mapping with improvements of 1.5-bit in peak effective number of bits (ENOB) and 9 dB in peak signal-to-noise-and-distortion ratio (SNDR) verified over three measured sample prototypes.

INDEX TERMS Analog-to-digital converter (ADC), time-based ADC, Dickson charge pump (CP), time quantization, voltage-to-time converter (VTC), ADC calibration, distortion correction.

I. INTRODUCTION

DESPITE the continual CMOS scaling in favor of higher speed and integration of digital circuitry, the reduction of transistor dimensions results in lowering of available voltage headroom, thus unavoidably causing deterioration of analog circuitry, such as ADCs. As gate length shrinks, shorter gate delay and therefore finer time resolution can be achieved in nanoscale CMOS. Instead of directly quantizing voltage/current information, ADC architectures which utilize time/frequency information could offer better solutions [1].

The time-domain approach can be exploited by means of a voltage-controlled oscillator (VCO) [2]. A VCO in such an ADC generates a clock whose frequency is proportional to the analog input voltage. The clock's phase is then sampled and differentiated such that the ADC's digital output is ideally proportional to the analog input. Unfortunately, the nonlinearity of the VCO's voltage-to-frequency conversion, which originates from the active devices, will directly affect the ADC's nonlinearity, thus requiring extensive calibration due to PVT variations [3].

An alternative time-domain ADC implementation is an intermediate conversion of the input analog voltage into time information using a voltage-to-time converter (VTC) prior to digitization using a time-do-digital converter (TDC) [4]–[8]. Most of the proposed topologies are, however, hardly amenable to a low supply voltage operation, given their analog-intensive implementation, i.e., operational transconductance amplifiers (OTAs) and current sources [4]. In [8], the compact nature of the inverter-based VTC presents a potential for high-speed time-based ADCs. In [9]–[13],

"hybrid" converters that make use of time-domain quantizers show promising performance but using analog intensive circuits brings limitations at finer CMOS nodes. In [13], a highly linear current source is required for a time-residue amplification. In order to increase the resolution in time-domain ADCs, a time amplifier is employed in [14]. However, complex calibration to correct the time amplifier's nonlinearity is necessary. Although [15], [16] demonstrated power-efficient time-domain data conversions using a linear current source for the time amplification without an expensive residue amplifier, there were restrictions in performance to either low bandwidth [15] or limited resolution [16]. In our previous work [17], we use a Dickson charge pump (CP) as a VTC but the system still needs a multitude of VTCs to overcome the non-linearity of the generated ramp signal. Event-based ADC in [18] can reduce the system sampling rate and power consumption but still requires analog comparators of high performance.

In this work, we propose a new architecture of a time-based ADC in which a sampled input voltage uses a reference ramp, generated by means of a Dickson CP, to produce a PWM signal whose width is inversely proportional to it. Thus realized voltage-to-time conversion (VTC) can be free from any highly linear current sources. The input-modulated pulse-width signal is fed into simple latches and digital logic for digital conversion. Due to the precise characteristics of Dickson CP, the digital outputs can be compensated through a deterministic digital mapping. At a nominal 1 V supply, the proposed ADC achieves a sample rate of 0.6 MS/s, while consuming 209 μW, in a highly digital implementation. The digital distortion correction is identical for all the measured samples and improves ENOB from 4.21 to 5.7 bits. Likewise, SNDR improves by up to 9 dB.

This article is organized as follows. Section II presents the proposed VTC exploiting Dickson charge pump and the distortion correction technique for linearizing its characteristics. Section III presents detailed implementation of the proposed ADC. Section IV describes measurement results.

II. DICKSON CHARGE-PUMP-BASED VOLTAGE-TO-TIME CONVERSION
In this section, we first study a working principle of the Dickson CP as a ramp reference signal generator for the proposed ADC. Then, top-level modeling and SPICE/MATLAB simulations of the effects of Dickson CP non-idealities are presented.

A. WORKING PRINCIPLE OF DICKSON CHARGE-PUMP
Dickson CP has been widely used in power management applications, in which a DC supply voltage, V_{DD}, is multiplied by a factor of N that is equal to the number of cascaded stages. Due to the charge-transfer operation of a Dickson multiplier, the steady-state output voltage V_S is a linear function of V_{DD}, and its time behavior can be well approximated by an RC exponential transient, increasing asymptotically towards V_S and with a time constant which depends on the
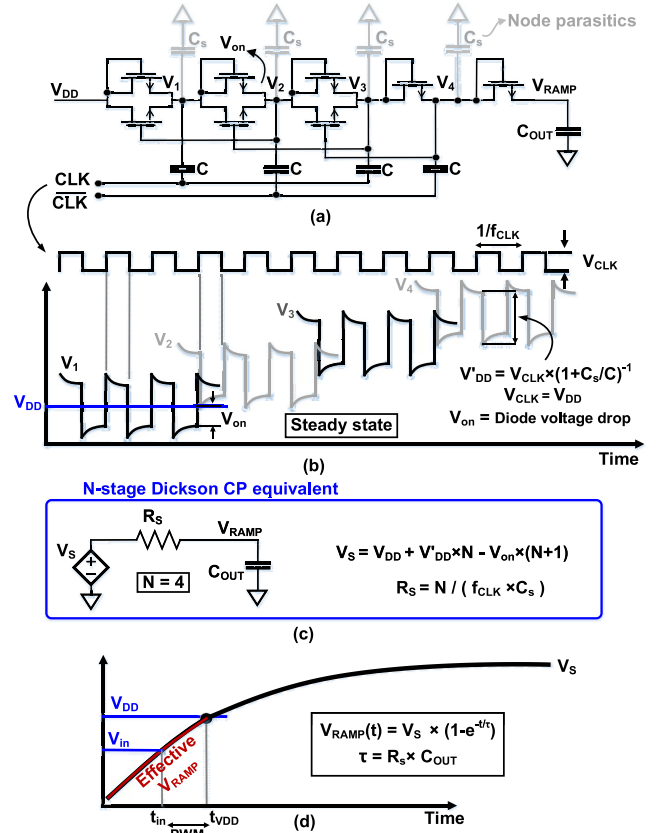

FIGURE 1. Dickson charge-pump: (a) schematic diagram ($N = 4$ for the sake of illustration), (b) corresponding waveforms, (c) equivalent model of (a), and (d) output voltage V_{ramp} vs. time.

CLK frequency (f_{CLK}), number of stages N and by the value of internal capacitance C. Thus, Dickson CP can operate as a voltage-slope generator which can be employed as a key building block in a VTC. Since it is composed of switches and capacitors, the proposed technique is suitable for highly scaled CMOS processes.

Figs. 1(a) and (b) show the schematic of Dickson charge-pump based on four cascaded stages and their corresponding signals, respectively. Each stage is composed of an NMOS switch in parallel to a diode-connected NMOS and a capacitor C. During the initial exponential transient, charge is transferred along the chain towards the output V_{ramp}. The voltages between each stage across the inter-staged capacitors (V_1 to V_4) are gradually charged as CLK signal of amplitude $V'_{DD} \approx V_{DD}$ is toggling at the bottom plates of inter-stage capacitors until their voltages reach their respective steady-state values of $V_{DD} - V_{on}$, $V'_{DD} + V_{DD} - 2V_{on}$, $2V'_{DD} + V_{DD} - 3V_{on}$, and $3V'_{DD} + V_{DD} - 4V_{on}$, where V_{on} is the voltage drop caused by the on-resistance of switches, and $V'_{DD} \approx V_{DD}$ is the voltage shift at each of the following nodes (V_1 to V_4) due to the clock switching action. V'_{DD} is slightly below V_{DD} (i.e., 1 V) as it is attenuated by the effect of parasitic capacitances from the switches. In this design, the supply rail voltage V_{DD} is tied to the CP input. Based on simulations of this 8-stage Dickson CP, V_S, which
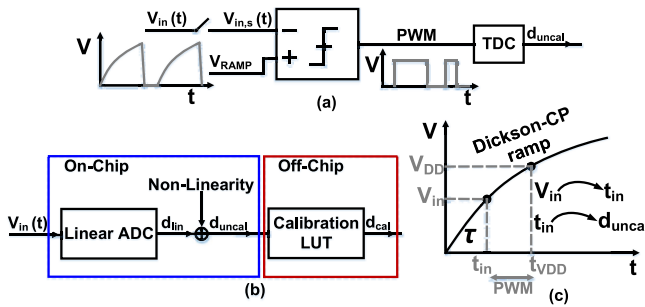
FIGURE 2. (a) Simplified diagram of the proposed time-domain Dickson CP ADC, (b) equivalent model, (c) generated ramp signal for a specific input analog voltage.
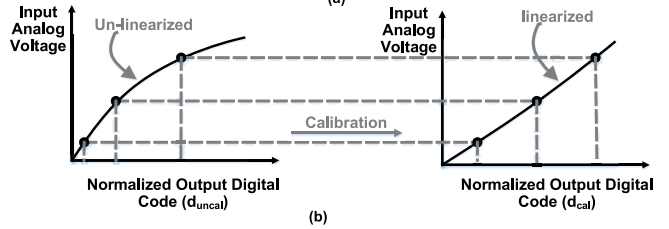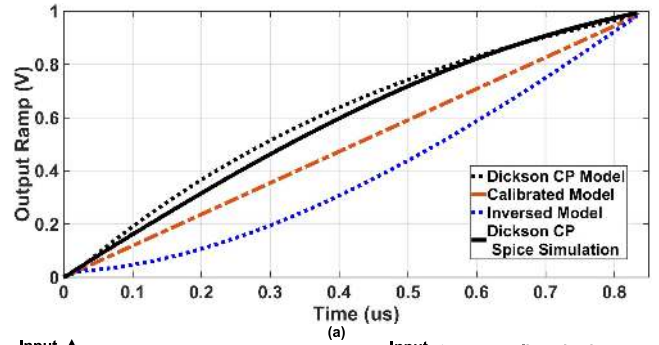

FIGURE 3. (a) Comparison of the theoretical modelling vs. simulated results of the derived reversed function of the voltage ramp generated from Dickson CP shown in (3) and the calibrated ramp derived in (5). (b) Digital post-processing to linearize Dickson CP characteristics.

is the steady-state output voltage of the Dickson CP, is estimated to be 5 V. V_4 transfers the generated voltage to V_{ramp} output through the last-stage switch. The overall waveform of V_{ramp} shown in Fig. 1(d) behaves as a charging ramp starting from 0 to V_S exceeding the supply voltage V_{DD}. Thanks to the proposed technique, it can be observed that the effective region from 0 to V_{DD} (shown in Fig. 1(d)) can exhibit better linearity as, for example, when using only a simple capacitor-resistor network that charges from zero to V_{DD}.

B. PROPOSED EQUIVALENT MODEL

As presented in the simplified model of the proposed system in Fig. 2(a), V_{ramp} generated by means of the Dickson CP is used as a reference to compare with samples $V_{in,s}$ of the input voltage $V_{in}(t)$. The output of comparator captures the timestamp t_{in} when V_{ramp} intersects with $V_{in,s}$ and it is further converted to digital domain by means of a TDC. Figure 2(b) shows the equivalent model of the ADC, consisting of a linear ADC that converts $V_{in}(t)$ to its equivalent normalized digital code d_{lin}, i.e., $0 \ldots V_{DD} \rightarrow 0 \ldots d_{max}$. By adding the non-linearity of the Dickson CP ramp signal, which is due to the exponential charge transfer characteristic of the Dickson CP, the equivalent model generates the final output digital code, d_{uncal}. In the second part of the model, the deterministic distortion correction look-up table (LUT), implemented off-chip, is used to compensate the non-linearity derived from the exponential charge characteristic of the Dickson CP.

Based on the derived model of the Dickson CP shown in Fig. 1(c), the generated ramp can be written as:

$$V_{ramp}(t) = V_S\left(1 - e^{-\frac{t}{\tau}}\right) \quad (1)$$

V_S is the steady-state equivalent voltage of the Dickson CP and τ represents the equivalent time-constant. Fig. 2(c) shows the generated CP ramp that maps the input signal V_{in} to its equivalent timestamp t_{in}. With an assumption that all the interface blocks, i.e., S&H and TDC, are ideal and the only source of non-linearity is the Dickson CP, t_{in} can be mapped as the un-calibrated digital code, i.e., d_{uncal} in Fig. 2(b).

$$V_{in} = V_S\left(1 - e^{-\frac{t_{in}}{\tau}}\right) \quad (2)$$

Due to the exponential/logarithmic mapping transfer function of V_{in} to t_{in} and then eventually to d_{uncal}, the latter has a logarithmic format:

$$d_{uncal} = K_{tdc} \cdot \tau \cdot \ln\left(\frac{V_S}{V_S - d_{lin}}\right) \quad (3)$$

Equation (3) derives from (2) by inserting d_{uncal} into t_{in} with a time-to-digital converter (TDC) gain [LSB/sec], K_{tdc}. It makes an assumption that the only source of non-linearity in the proposed model is from the Dickson CP. As a result, t_{in} can be mapped into the normalized output digital code. Therefore, the linearized CP ramp signal can be derived from (3) as:

$$d_{cal} = V_S\left(1 - e^{-\frac{d_{uncal}}{K_{tdc} \cdot \tau}}\right) \quad (4)$$

where d_{cal} represents the final output code after the aforementioned distortion correction method. Following this approach, the correction LUT can be derived from the inverse of known characteristics of the Dickson CP, and implemented fully in the digital domain. If the nonlinear characteristic of Dickson CP can correctly match the proposed digital mapping, the normalized output code will be fully calibrated and so the output code will be linearized as follows:

$$d_{cal}(d_{uncal}) = d_{lin} \quad (5)$$

as a result of inserting (3) into (4).

Figure 3(a) shows simulation results of the normalized output signal of the Dickson CP vs. time. The CP of Fig. 1(a) is designed in 28 nm CMOS with $N = 8$ stages. It runs at f_{CLK} of 400 MHz. Capacitors C_{out} and C are 2 pF and 30 fF, respectively. The critical node in terms of noise is the input of the VTC which has a smaller capacitor (i.e., C). By choosing 30 fF, the equivalent KT/C noise will be $<400\,\mu$Vrms,
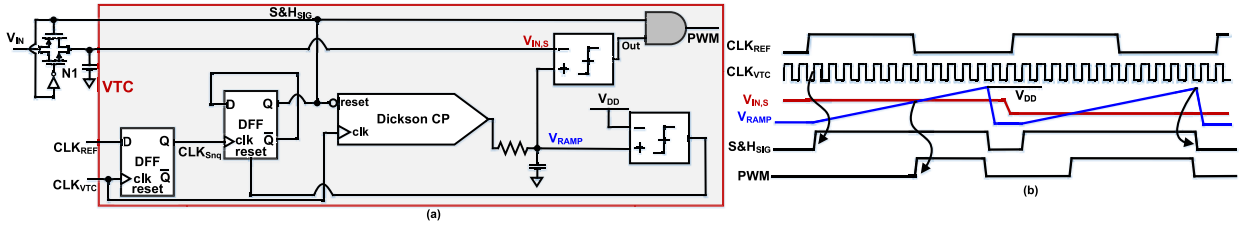
FIGURE 4. (a) Detailed schematic of the proposed voltage-to-time converter (VTC) exploiting Dickson charge pump and pulse-width modulator. (b) Timing diagram and corresponding waveforms.

which is sufficient for the required design specifications. Comparison of the results from theoretical modelling (with reference to (2), (3) and (5)) vs. simulated results of the derived reversed function of the CP voltage ramp shown in (4) and the calibrated ramp derived in (5) are also shown in Fig. 3(a). It can be observed that the simulation results for the implemented Dickson CP are in compliance with the derived model. The inverse and calibrated characteristics of the proposed technique are extracted from the previously derived (3) and (4).

The ramp generated by the CP is used as a reference to a comparator for pulse-width modulated output as it is compared to the sampled input voltage. To compensate for the CP non-linearity effects, the generated ramp signal (V_{ramp}) and its corresponding inverse function are combined to generate the calibrated ramp signal, which can be accurately pre-determined. Based on (4), a deterministic LUT is constructed to represent d_{cal} and nonlinear digital output codes can be corrected as shown in Fig. 3(b).

III. PROPOSED ARCHITECTURE
A. HARDWARE ARCHITECTURE
Fig. 4 illustrates a detailed diagram of the Dickson-CP-based voltage-to-time converter (VTC) used in the proposed time-domain ADC. The CP is composed of $N = 8$ stages. This helps improving the linearity of V_{ramp} as higher N results in increased V_S, as illustrated in Fig. 1. Furthermore, smaller C_{out} results in weaker filtering of the generated ramp. This can effect the ADC performance by increasing the ripple on the Dickson CP output due to its high-frequency clocking. A faster CP clock, CLK_{VTC}, results in lower t_{vdd}, allowing to use a faster ADC sampling clock, CLK_{REF}, but it also leads to higher power consumption while requiring more sensitive TDC due to the steeper slope of the generated ramp.

The CLK_{REF} and CLK_{VTC} signals terminate on the D-flip-flop (DFF) to generate a synchronized clock, CLK_{Snq}, which enables PWM and eventually resets all the Dickson CP capacitors when the generated ramp signal reaches V_{DD}. The CP is clocked at 400 MHz by CLK_{VTC}. As it is toggling, output voltage V_{ramp} keeps on increasing. The time at which V_{ramp} crosses the sampled input signal, i.e., $V_{IN,S}$ will trigger the PWM pulse. At a later instance when the ramp signal V_{ramp} crosses over V_{DD}, the output of the following latch comparator, in turn, triggers the reset of the Dickson CPs by shorting to ground their V_{1-8} internal nodes (shown in
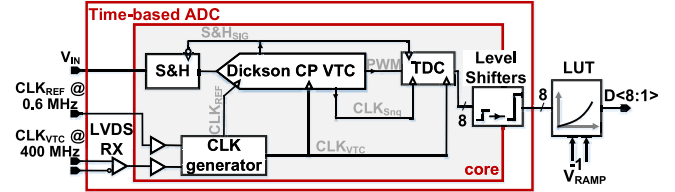
Fig. 1), until the next CLK_{Snq} rising edge in order to avoid further increase in the V_{ramp} which can damage the devices. $S\&H_{SIG}$ feeds the AND gate to generate the falling edge of the PWM's signal and is also being used as a controlling signal for the active-low S&H circuit in the proposed ADC. The falling edge of the PWM signal is being controlled not by the sampled input analog signal ($V_{IN,S}$) but by the discharging signal of the Dickson CP (i.e., $S\&H_{SIG}$), in order to avoid intermodulation with the input analog signal which can increase the noise. Fig. 4(b) shows more details of the timing behavior of the controlling signal of the proposed ADC.

The detailed diagram of the proposed top-level architecture is shown in Fig. 5. It is composed of the core ADC operating at $V_{DD} = 1$ V, an LVDS receiver for the Dickson CP clock (CLK_{VTC}), output voltage level shifters for transmitting the output code $D < 8:1 >$ to the off-chip data acquisition and off-chip digital mapping which linearizes the un-calibrated output code, as discussed in Section II. The core circuit is composed of the Dickson CP as VTC, sample and hold circuit (S&H), clock generator block, and TDC.

Fig. 6 reveals the schematic of the TDC which comprises an asynchronous 8-bit counter. It starts counting at the rising edge of PWM until the next rising edge of CLK_{Snq}. The generated quantized digital output $D < 8:1 >$ bus will be sent to the level shifter at the falling edge of $S\&H_{SIG}$, while the counter still keeps counting, which helps relaxing the timing constraint between the counter resetting and data transferring phases, as shown at the bottom of Fig. 6.

B. DESIGN PROCESS
As shown in Fig. 1(c), increasing the number of stages, N, can result in a higher steady-state voltage V_S. From Fig. 1(d), higher V_S leads to a more linear ramp within the effective region spanning from the ground to the nominal supply voltage V_{DD}. This leads to a more accurate voltage-to-time
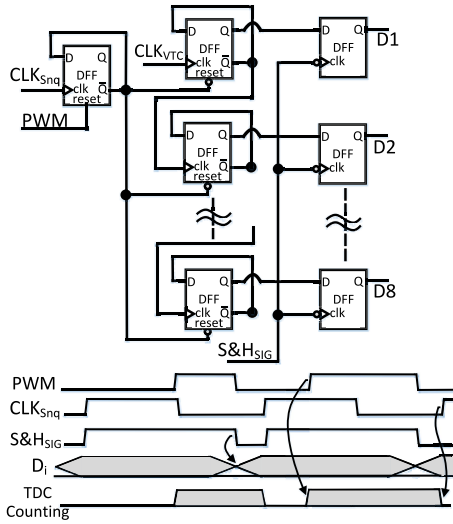

FIGURE 5. Detailed diagram of the proposed time-mode ADC.

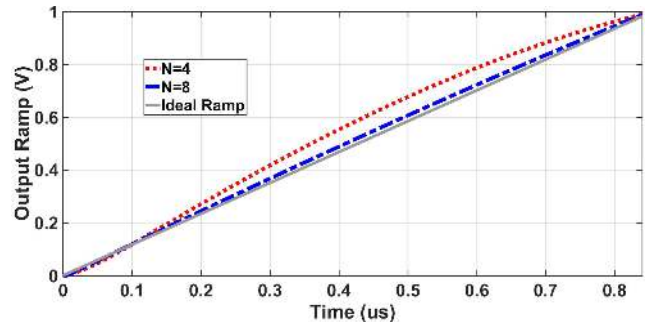FIGURE 6. Detailed schematic of TDC and corresponding timing diagram.

FIGURE 7. Comparison between an ideal ramp with the normalized simulation results for the ramp generated by Dickson CP circuit utilizing N of 4 and 8.
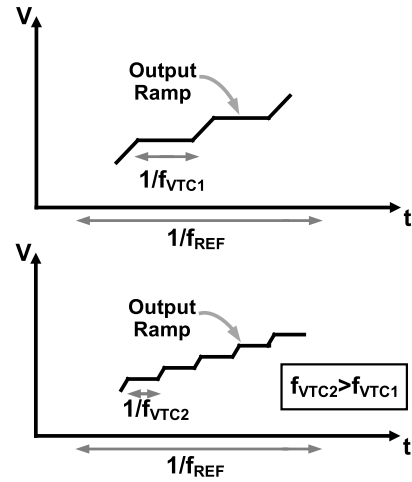

FIGURE 8. Quantization error in the Dickson CP ramp signal as a function of f_{VTC}.

conversion and ultimately to a more faithful PWM. To prove the concept described above, the time-domain equation of the generated ramp signal is derived as follows. From (1), assuming V_{on} is negligible, as well as the peak-to-peak voltage of the clock buffers is equal to V_{DD}, V_{ramp} can be derived as:

$$V_{ramp}(t) = (N+1)V_{DD}\left(1 - e^{\frac{-t}{R_S C_{out}}}\right) \qquad (6)$$

Assuming, $V_{ramp}(t)$ reaches V_{DD} at time $t = t_{vdd}$, as shown in Fig. 1(d), (6) can be re-written as:

$$R_S \cdot C_{out} = \frac{t_{vdd}}{\ln\left(1 + \frac{1}{N}\right)} \qquad (7)$$

For a fair comparison of the V_{ramp} linearity, we adjust C_{out} such that V_{DD} is reached at the same t_{vdd} across all different cases of N. The deviation $V_{err}(t)$ of the generated ramp from the ideal linear ramp can be calculated as:

$$V_{err}(t) = (N+1)V_{DD}\left(1 - e^{\frac{-t}{R_S C_{out}}}\right) - \frac{V_{DD} \cdot t}{t_{vdd}} \qquad (8)$$

The instantaneous voltage error during $t = 0 \ldots t_{vdd}$ can be re-written by substituting (7) into (8):

$$V_{err}(t) = (N+1) \cdot V_{DD} \cdot \left(1 - \left(\frac{N+1}{N}\right)^{\frac{-t}{t_{vdd}}}\right) - \frac{V_{DD} \cdot t}{t_{vdd}} \qquad (9)$$

It can be observed that by adjusting C_{out} for the ramp to hit V_{DD} at t_{vdd}, the case of utilizing a larger number of stages (e.g., $N = 8$) will result in better linearity than when N is lower (e.g., $N = 4$). This is illustrated in Fig. 7, which compares the ideal ramp with the ramps generated with $N = 4$ and 8 based on SPICE simulations in this TSMC 28 nm LP CMOS technology.

By utilizing a higher frequency f_{CLK} of clock CLK_{VTC} to quickly reach the desired voltage level at the output of the Dickson CP, as described in Fig. 1(c), a faster sampling rate

can be achieved. However, the higher sampling rate entails higher charging current with wider switching transistors as to reduce the on-resistance. Unfortunately, the larger transistors also increase the parasitic capacitance, ultimately resulting in larger voltage losses in the switches [19]. Additionally, the high-frequency clocking driving the capacitors in the Dickson CP (i.e., C in Fig. 1) may generate ripples at the output due to the AC coupling from the clock generator to the Dickson CP output capacitor (i.e., C_{out}), deteriorating the linearity of the generated ramp signal. To avoid these issues, an appropriate ratio between the frequencies of CLK_{VTC} and CLK_{REF} should be carefully defined to achieve the targeted ADC resolution (N_{ADC}) within the corresponding input range (V_{range}).

Fig. 8 illustrates how the quantization effects at the output ramp of the Dickson CP can be lowered by increasing f_{VTC}. The quantization step is a function of a time step at the pumping stages which is inversely proportional to f_{VTC}. Assuming the same slope of the generated ramps, the quantization steps can be finer with increased f_{VTC}. To achieve this goal, the ratio of f_{VTC} over f_{REF} must be much higher than the total number of voltage steps within the range of the ADC convergence time. Unfortunately, this will lead to a difficult tradeoff with the efficiency of the CP switches

and can contribute to unnecessary high power consumption. A condition to minimize the quantization effects caused by the high frequency clock can be written as:

$$\frac{f_{\text{VTC}}}{f_{\text{REF}}} \gg \left(\frac{V_{\text{DD}}}{V_{\text{range}}} \times 2^{N_{\text{ADC}}} \right) \qquad (10)$$

By plugging in into (10) the design numbers ($f_{\text{VTC}} = 400$ MHz, $f_{\text{REF}} = 0.6$ MHz, $V_{\text{DD}} = 1$ V and $V_{\text{range}} = 0.3$ V, and $N_{\text{ADC}}=6$ bits), assuming that the analog input voltage range is one-third of V_{DD}, we obtain (11) that meets the design specifications.

$$\frac{400\text{MHz}}{0.6\text{MHz}} \gg \left(\frac{1V}{0.3V} \times 2^6 \right) \qquad (11)$$

On the other hand, the TDC comprises the DFF counter which counts the number of CLK_{VTC} edges within the period of pulse generated (i.e., PWM) by the prior-stage Dickson CP VTC. As a result, the frequency of CLK_{VTC} should be chosen such that the TDC gain matches with the maximum range of PWM. To meet the required specification, it can be written as:

$$\frac{V_{\text{range}}}{V_{\text{DD}}} \times \frac{f_{\text{VTC}}}{f_{\text{REF}}} < 2^{N_{\text{TDC}}} \qquad (12)$$

In this design, it can be shown that the condition can be met as:

$$\frac{0.3V}{1V} \times \frac{400\text{MHz}}{0.6\text{MHz}} < 2^8 \qquad (13)$$

It can be concluded that the given specifications meet the system design requirements for the resolution of the TDC (i.e., N_{TDC}).

Regarding the noise requirements, there are two separate parts to consider, i.e., kT/C noise of the capacitors in the Dickson CP at 1) the output capacitance C_{out}, and 2) the pumping capacitors in the intermediate stages (i.e., C), see Fig. 1. The sum of these two noise contributions must satisfy the SNR requirements of the system. Assuming $C_{\text{out}} = 2$ pF and $C = 30$ fF, the thermal noise budget for each section can be calculated as $45\,\mu V_{rms}$ and $370\,\mu V_{rms}$, respectively, which is much smaller than the target specification, i.e., 4.6 mV LSB ($N_{\text{ADC}} = 6$, and $V_{\text{range}} = 300$ mV). Note that the noise of the charge pump circuit is limited by the output capacitor, i.e., C_{out}, as described in [20]. A similar conclusion was obtained in [21] for a re-programmable switched-capacitor filter with a complex network of capacitors.

As far as the jitter requirement is concerned, Fig. 9 plots the conceptual diagram of the generated ramp from the Dickson CP VTC in the interval of $t = 0 \ldots t_{\text{vdd}}$. It can be observed that the timing error or jitter (Δt_{error}) of the high frequency clock CLK_{VTC} can be translated into voltage noise. Assuming a linear characteristics of the generated ramp, the slope can be written as $V_{\text{DD}}/t_{\text{vdd}}$. To avoid the jitter affecting the targeted ADC resolution (N_{ADC}), the equivalent voltage error should be less than 1 LSB. For $N_{\text{ADC}} = 6$, the condition can be written as:

$$\Delta t_{\text{err}} \ll V_{\text{LSB}} \times \frac{t_{\text{vdd}}}{V_{\text{DD}}} \qquad (14)$$
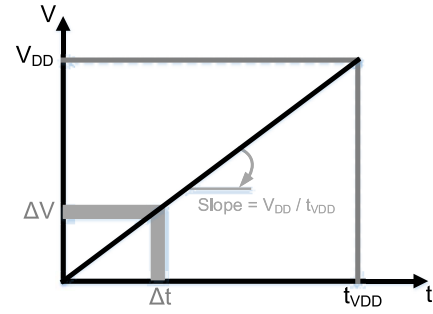

FIGURE 9. Dickson CP ramp signal with the effects of timing error of CLK_{VTC} leading to the voltage error.
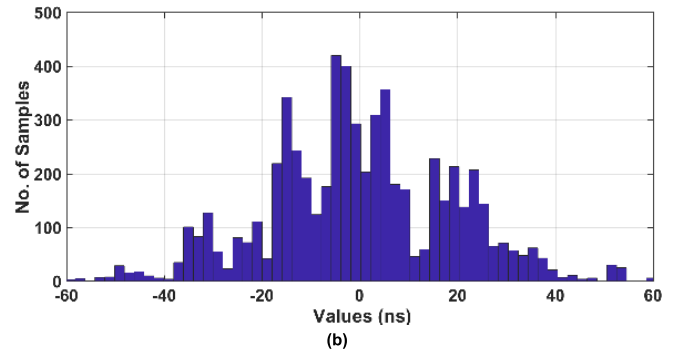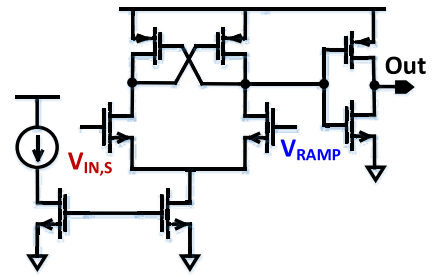

FIGURE 10. VTC comparator: (a) schematic, (b) SPICE Monte Carlo simulation result of the comparator's time offset.

By inserting the targeted performance into (14), it can be ascertained that the timing error of CLK_{VTC} should be less than 7.9 ns.

Fig. 10 shows the 500-run Monte Carlo circuit-level simulation of the comparator's timing offset. The standard deviation (STD) of the timing offset reads 19 ns. Since it is constant and independent of the input, the comparator delay will merely add a constant timing offset equally for all the generated PWMs. Hence, the system linearity will not be affected.

IV. MEASUREMENT RESULTS
The microphotograph of the proposed ADC is shown in Fig. 11. It is fabricated in TSMC LP 28 nm CMOS and occupies 0.04 mm^2. The total consumed power at the maximum conversion rate of 0.6 MS/s is 209 μW, including input buffers and output voltage-level-shifters. The consumed power is broken down as: 25% for the clock buffer, 60% for the VTC, including the comparators and the Dickson CP, and 15% for the TDC and the level-shifter.
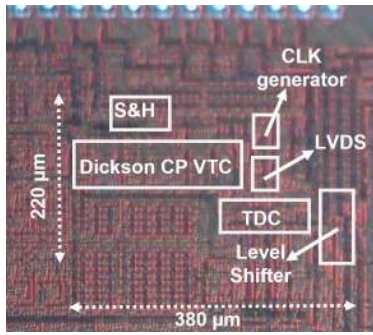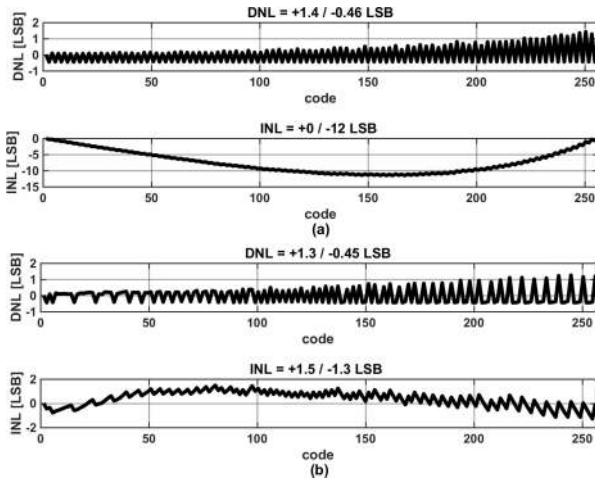
FIGURE 11. Die microphotograph.

FIGURE 12. DNL/INL measurement results: (a) before distortion correction, and (b) after distortion correction.
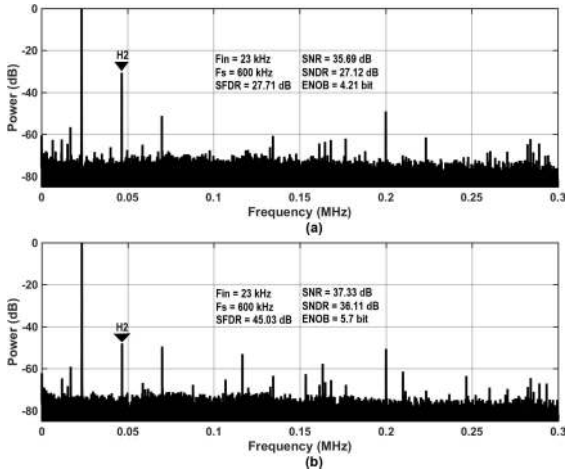

FIGURE 13. Dynamic characterization measurement result for f_{in} = 23 kHz, (a) before distortion correction, (b) after distortion correction.

FIGURE 14. Dynamic characterization measurement results for f_{in} = 293 kHz: (a) before distortion correction, and (b) after distortion correction.

FIGURE 15. Dynamic variation vs. input frequency: (a) before distortion correction, and (b) after distortion correction.

The static linearity characterized at the 1 V nominal supply, 0.6 MS/s sampling rate and using a 3 kHz input sine-wave is shown in Fig. 12, demonstrating a differential (DNL) and integral nonlinearity (INL), respectively, equal to $+1.3/-0.45$ LSB, and $+1.5/-1.3$ LSB, after the correct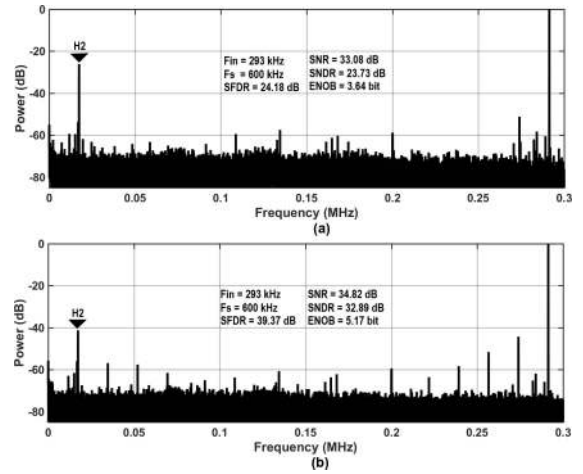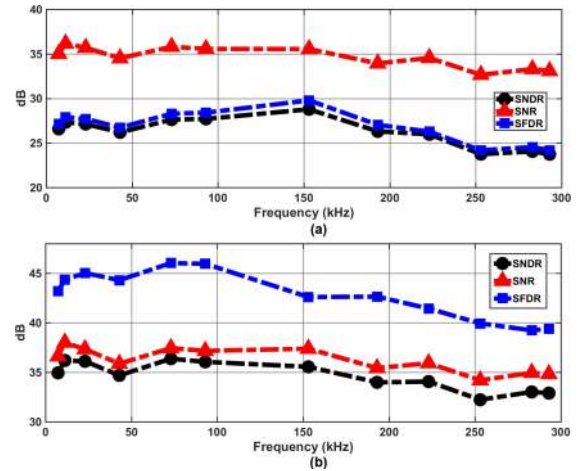ion. The dynamic linearity characterization of the converter is presented in Figs. 13 and 14, before and after the distortion correction, respectively. Two input frequency cases are applied: low-frequency (23 kHz) input sine-wave and a near-Nyquist 0.293 MHz at the maximum conversion rate of 0.6 MS/s. Note that matching of coefficients in the LUT could partially cancel out the second harmonic, but for the higher harmonics the task would be much more challenging due to the mismatch between LUT and process variation in the fabricated chip.

Fig. 15 shows the measured SFDR, SNR and SNDR across the sine-wave input frequency. The SNDR characterization over three different IC chips at 0.6 MS/s sampling frequency is shown in Fig. 16. Less than 15% performance variation can be observed, which indicates the robustness of our approach. Fig. 15 shows almost 15 dB improvement in the SFDR after the distortion correction, which is due to the suppression of the second harmonic of the output power spectrum, as shown in Figs. 13 and 14.

VOLUME 2, 2021   29

TABLE 1. Comparison table of state-of-the-art time-domain ADCs.

	LIn, JSSC'15	Wang, TCASII'09	Danesh, JSSC'13	Shen, TCASII'11	Chen, VLSI'16	Straayer, VLSI'07	Song, JSSC'00	Wang, JSSC'09	This Work
Architecture	Pipeline	ZCBC Time Domain	Time-interleaved	CP Pipeline	Two-stepTD	CT Delta-Sigma	Current Interpolate	Pipelined	Dickson-CP Time Domain
Technology	90	180	130	90	180	130	350	350	28
SamplingRate (MHz)	160	20	250	100	3.4	40	50	40	0.6
SNDR (dB)	37.88	44.2	49.95	37.1	59.1	55	27	70.2	36.11
ENOB	6	7.04	8.0	5.8	9.5	8.8	4.2	11.4	5.7
FoM (pJ/c-s)	0.23	1.76	0.40	0.25	1.16	2.13	10.9	4.4	6.70
Power (mW)	2.43	4.64	25.3	1.39	2.9	38.0	10	231	0.21
Area (mm²)	0.25	0.84	0.55	0.04	0.07	0.19	4.8	7.5	0.04
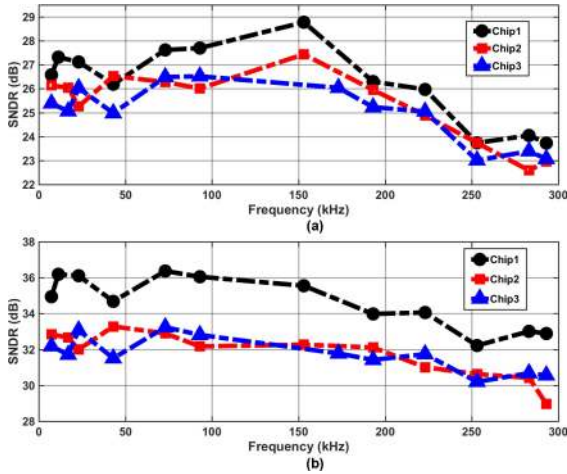
FIGURE 16. SNDR variation for three different samples vs. input frequency: (a) before distortion correction, (b) after distortion correction.

The generated LUT, based on the proposed model and equation, was kept identical for all the three measured samples. It shows almost an identical performance improvement for all the three samples. Table 1 summarizes the ADC performance after the correction and compares it with state-of-the-art time-domain (TD) ADCs. The ADC achieves more than 1.5-bit and 9-dB improvement in ENOB and SNDR, respectively, thanks to the proposed affordable and digital friendly distortion correction technique to linearize the predictable non-linearity of the designed passive Dickson-CP-based VTC. Without any use of analog-intensive circuits for the VTC ramp generation, the proposed ADC can achieve good SNDR among state-of-the-art TD ADCs under a lower power consumption.

V. CONCLUSION
This article presents a time-based ADC employing a Dickson charge-pump (CP) for the purpose of ramp generation in a voltage-to-time conversion (VTC). The proposed ADC

makes use of a well-behaved transient behavior of the Dickson CP to generate a ramp signal as a VTC and transmitting the modulated signal to a TDC for quantization. Using the Dickson CP as a VTC can potentially relieve various types of ADCs from using intensive analog circuits, such as current sources or OTAs, which can be rather challenging in advanced CMOS nodes. The proposed distortion correction technique generates look-up table values without any need for individual fine-tuning.
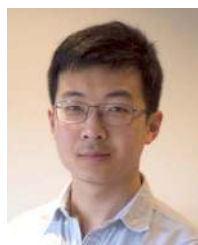
REFERENCES
[1] R. B. Staszewski, S. Vemulapalli, P. Vallur, J. Wallberg, and P. T. Balsara, "1.3 V 20 ps time-to-digital converter for frequency synthesis in 90-nm CMOS," *IEEE Trans. Circuits Syst. II, Exp. Briefs*, vol. 53, no. 3, pp. 220–224, Mar. 2006.

[2] B. Young *et al.*, "A 75 dB DR 50 MHz BW 3rd order CT-ΔΣ modulator using VCO-based integrators," in *Symp. VLSI Circuits Dig. Tech. Papers*, 2014, pp. 1–2.

[3] V. Nguyen, F. Schembari, and R. B. Staszewski, "A 0.2-V 30-MS/s 11b-ENOB open-loop VCO-based ADC in 28-nm CMOS," *IEEE Solid-State Circuits Lett.*, vol. 1, no. 9, pp. 190–193, Sep. 2018.

[4] S. Naragh *et al.* "A 9-bit, 14 uW and 0.06 mm² pulse position modulation ADC in 90 μm digital CMOS," *IEEE J. Solid-State Circuits*, vol. 45, no. 9, pp. 1870–1880, Sep. 2010.

[5] S. Zhu, B. Xu, B. Wu, K. Soppimath, and Y. Chiu, "A skew-free 10 GS/s 6 bit CMOS ADC with compact time-domain signal folding and inherent DEM," *IEEE J. Solid-State Circuits*, vol. 51, no. 8, pp. 1785–1796, Aug. 2016.

[6] Y. M. Tousi and E. Afshari, "A miniature 2 mW 4 bit 1.2 GS/s delayline-based ADC in 65 nm CMOS," *IEEE J. Solid-State Circuits*, vol. 46, no. 10, pp. 2312–2325, Oct. 2011.

[7] M. Miyahara, I. Mano, M. Nakayama, K. Okada, and A. Matsuzawa, "22.6 A 2.2 GS/s 7 b 27.4 mW time-based foldingflash ADC with resistively averaged voltage-to-time amplifiers," in *IEEE Int. Solid-State Circuits Conf. (ISSCC) Dig. Tech. Papers*, 2014, pp. 388–389.

[8] Y. Xu, G. Wu, L. Belostotski, and J. W. Haslett, "A 5 GS/s 4-bit time-based single-channel CMOS ADC for radio astronomy," in *Proc. IEEE Custom Integr. Circuits Conf. (CICC)*, 2013, pp. 1–4.

[9] C.-H. Weng, T.-A. Wei, E. Alpman, C.-T. Fu, Y.-T. Tseng, and T.-H. Lin, "An 8.5 MHz 67.2 dB SNDR CTDSM with ELD compensation embedded twin-T SAB and circular TDC-based quantizer in 90 nm CMOS," in *Symp. VLSI Circuits Dig. Tech. Papers*, 2014, pp. 1–2.

[10] Y. Chen and C. Hsieh, "A 0.4 V 2.02 fJ/conversion-step 10-bit hybrid SAR ADC with time-domain quantizer in 90 nm CMOS," in *Symp. VLSI Circuits Dig. Tech. Papers*, 2014, pp. 1–2.

[11] C. S. Taillefer and G. W. Roberts, "Delta–sigma A/D conversion via time-mode signal processing," *IEEE Trans. Circuits Syst. I, Reg. Papers*, vol. 56, no. 9, pp. 1908–1920, Sep. 2009.

[12] J. P. Mathew, K. Long, and B. Razavi, "A 12-bit 200-MS/s 3.4-mW CMOS ADC with 0.85-V supply," in *Symp. VLSI Circuits Dig. Tech. Papers*, 2015, pp. C66–C67.

[13] T. Oh, H. Venkatram, and U.-K. Moon, "A 70MS/s 69.3 dB SNDR 38.2fJ/conversion-step time-based pipelined ADC," in *Symp. VLSI Circuits Dig. Tech. Papers*, 2013, pp. 96–97.

[14] T. Oh, H. Venkatram, and U.-K. Moon, "A time-based pipelined ADC using both voltage and time domain information," *IEEE J. Solid-State Circuits*, vol. 49, no. 4, pp. 961–971, Apr. 2014.

[15] H. Y. Yang and R. Sarpeshkar, "A time-based energy-efficient analog-to-digital converter," *IEEE J. Solid-State Circuits*, vol. 40, no. 8, pp. 1590–1601, Aug. 2005.

[16] J. Shen and P. R. Kinget, "Current-charge-pump residue amplification for ultra-low-power pipelined ADCs," *IEEE Trans. Circuits Syst. II, Exp. Briefs*, vol. 58, no. 7, pp. 412–416, Jul. 2011.

[17] A. Esmailiyan, F. Schembari, and R. B. Staszewski, "A 0.36-V 5-MS/s time-mode flash ADC with Dickson-charge-pump-based comparators in 28-nm CMOS," *IEEE Trans. Circuits Syst. I, Reg. Papers*, vol. 67, no. 6, pp. 1789–1802, Jun. 2020.

[18] H. Wang, V. Nguyen, F. Schembari, and R. B. Staszewski, "An adaptive-resolution quasi-level-crossing delta modulator with VCO-based residue quantizer," *IEEE Trans. Circuits Syst. II, Exp. Briefs*, vol. 67, no. 12, pp. 1–5, Dec. 2020.

[19] T. Tanzawa, "A switch-resistance-aware dickson charge pump model for optimizing clock frequency," *IEEE Trans. Circuits Syst. II, Exp. Briefs*, vol. 58, no. 6, pp. 336–340, Jun. 2011.

[20] I. Yousr, "High-voltage generation and drive in low-voltage CMOS technology," Ph.D. dissertation, Dept. Elect. Eng., Tech. Univ. California, Los Angeles, CA, USA, 2015. [Online]. Available: https://escholarship.org/content/qt7g1014zm/qt7g1014zm.pdf?t=nrzmjc

[21] M. Tohidian, I. Madadi, and R. B. Staszewski, "Analysis and design of a high-order discrete-time passive IIR low-pass filter," *IEEE J. Solid-State Circuits*, vol. 49, no. 11, pp. 2575–2587, Nov. 2014.

ALI ESMAILIYAN was born in Isfahan, Iran, in 1990. He received the B.Sc. degree in microelectronics from the Isfahan University of Technology, Isfahan, in 2013, and the M.Sc. degree in microelectronics from the University of Tehran, Tehran, Iran, in 2016. He is currently pursuing the Ph.D. degree in microelectronics with University College Dublin, Dublin, Ireland. In 2017, he joined Equal1, Fremont, CA, USA, as an IC Design Intern. His current research interests include time-based ADCs and cryogenic mixed-signal circuit design for quantum computer applications.

JIANGLIN DU (Member, IEEE) was born in Changchun, China, in 1990. He received the B.Sc. degree in microelectronics and the M.Sc. degree in physical electronics from Jilin University, Changchun, in 2013 and 2016 respectively. He is currently pursuing the Ph.D. degree in mixed-signal integrated circuit design with University College Dublin, Dublin, Ireland. His current research interests include low-power frequency synthesizer design, low-power receiver design, grating coupler for silicon-photonic, and cryogenic circuit design for quantum computer applications.

TEERACHOT SIRIBURANON (Senior Member, IEEE) received the B.E. degree in telecommunications engineering from the Sirindhorn International Institute of Technology, Thammasat University, Pathumthani, Thailand, in 2010, and the M.E. and Ph.D. degrees in physical electronics from the Tokyo Institute of Technology, Tokyo, Japan, in 2012 and 2016, respectively.

In 2016, he joined University College Dublin (UCD), Dublin, Ireland, as a Postdoctoral Researcher under the Marie Skłodowska-Curie Individual Fellowship Program. Since 2019, he has been an Assistant Professor with UCD. His research interests are CMOS wireless transceiver systems and clock/frequency generations for wireless and wireline communications. He was a recipient of the Japanese Government (MEXT) Scholarship, the Young Researcher Best Presentation Award at Thailand–Japan Microwave in 2013, the ASP-DAC Best Design Award in 2014 and 2015, the IEEE SSCS Student Travel Grant Award in 2014, the IEEE SSCS Predoctoral Achievement Award in 2016, and the Tejima Research Award in 2016. He has been a Guest Editor for IEEE TRANSACTIONS ON CIRCUIT AND SYSTEMS—PART I: REGULAR PAPERS and serves as a Reviewer for the IEEE JOURNAL OF SOLID-STATE CIRCUITS.

FILIPPO SCHEMBARI (Member, IEEE) was born in Codogno, Italy, in 1988. He received the B.Sc. degree in biomedical engineering in 2010, and the M.Sc. and Ph.D. degrees in electrical engineering from the Politecnico di Milano, Milan, Italy, in 2012 and 2016, respectively.

He worked on low-noise multichannel readout ASICs for X- and γ-ray spectroscopy and imaging applications. From 2016 to 2019, he worked as a Postdoctoral Researcher with University College Dublin, Ireland, focusing on deep-subthreshold time-mode ADCs, level-crossing-sampling ADCs, mismatch-calibrated SAR ADCs, and SAR TDCs. During this period, he also worked for six months as an IC Design Intern with Xilinx, Dublin. In 2019, he joined Huawei Technologies, Milan, Italy, as an Analog IC Designer. He was a recipient of the 2018 IEEE Emilio Gatti and Franco Manfredi Best Ph.D. Thesis Award in Radiation Instrumentation, and the Marie Skłodowska-Curie European Individual Fellowship in 2017.

ROBERT BOGDAN STASZEWSKI (Fellow, IEEE) was born in Bialystok, Poland. He received the B.Sc. (*summa cum laude*), M.Sc., and Ph.D. degrees in electrical engineering from the University of Texas at Dallas, Richardson, TX, USA, in 1991, 1992, and 2002, respectively.

From 1991 to 1995, he was with Alcatel Network Systems, Richardson, involved in SONET cross-connect systems for fiber-optic communications. He joined Texas Instruments Inc., Dallas, TX, USA, in 1995, where he was elected as a Distinguished Member of Technical Staff (limited to 2% of technical staff). From 1995 to 1999, he was engaged in advanced CMOS read channel development for hard disk drives. In 1999, he co-started the Digital RF Processor (DRP) Group within Texas Instruments with a mission to invent new digitally intensive approaches to traditional RF functions for integrated radios in deeply scaled CMOS technology. He was appointed as a CTO of the DRP Group from 2007 to 2009. In 2009, he joined the Delft University of Technology, Delft, The Netherlands, where he currently holds a guest appointment of Full Professor (*Antoni van Leeuwenhoek Hoogleraar*). Since 2014, he has been a Full Professor with University College Dublin, Dublin, Ireland. He is also the Co-Founder of a startup company, Equal1 Labs, with design centers located in Silicon Valley and Dublin, aiming to produce single-chip CMOS quantum computers. He has authored or coauthored five books, seven book chapters, 120 journal and 200 conference publications, and holds 200 issued U.S. patents. His research interests include nanoscale CMOS architectures and circuits for frequency synthesizers, transmitters and receivers, as well as quantum computers. He was a recipient of the 2012 IEEE Circuits and Systems Industrial Pioneer Award. In May 2019, he received the title of Professor from the President of the Republic of Poland. He was the TPC Chair of 2019 ESSCIRC in Kraków, Poland.